Circulating Harmonic Currents Suppression of Level-Increased NLM Based Modular Multilevel Converter With Deadbeat Control

Xingxing Chen, *Student Member, IEEE*, Jinjun Liu, *Fellow, IEEE*, Shuguang Song, *Student Member, IEEE*, and Shaodi Ouyang, *Member, IEEE*

***Abstract*—This article first analyzes the effect of the level-increased nearest level modulation (NLM) to the circulating current of the modular multilevel converter (MMC). The total inserted submodule (SM) number in one phase-leg of the MMC is variable using the level-increased NLM, which can significantly increase the peak-to-peak value of the circulating harmonic currents. Then, a circulating harmonic currents suppression method is proposed by applying deadbeat control for the MMC with level-increased NLM. Compared with the existing direct circulating current control approaches for the MMC, the proposed method presents specific extension and adjustment principle of the total inserted SM number. Therefore, the proposed method can improve the dynamic control performance and handle large circulating harmonic currents at steady state. And it can well coordinate the modulation and circulating harmonic currents suppression stages to avoid disturbing the ac-side output voltage while regulating the circulating current. The effectiveness of the proposed method is evaluated by a single-phase industrial-level simulated MMC system and a laboratory experimental platform.**

***Index Terms*—Circulating harmonic currents, deadbeat control, modular multilevel converter (MMC), nearest level modulation (NLM).**

NOMENCLATURE

N	SM number per arm.
L	Inductance in each arm.
C	SM capacitance.
U_c	Capacitor voltage.
$U_{\rm dc}$	Dc source voltage of the MMC.
$R_{\rm o}$	Load resistance.
$L_{\rm o}$	Load inductance.
$u_{\rm o}$	Load voltage.
$i_{\rm o}$	Output current.
$i_{\rm cir}$	Circulating current.
$i^*_{\rm cir}$	Reference of the circulating current.
i_u	Upper arm current.
i_l	Lower arm current.
$i_{\rm dc}$	Dc component of the circulating current.
i_h	Harmonic components of the circulating current.
u_Δ	Difference of the arm voltages.
$u^*_\Delta/2$	Reference of the ac-side output voltage.
$u_\sum$	Summation of the arm voltages.
$u^*_\sum$	Reference of $u_\sum$.
u_u	Upper arm voltage.
u^*_u	Reference of the upper arm voltage.
u_l	Lower arm voltage.
u^*_l	Reference of the lower arm voltage.
n_u	Upper arm inserted SM number.
n_l	Lower arm inserted SM number.
$U_{\rm cu\_ave}$	Average value of the upper arm capacitor voltages.
$U_{\rm cl\_ave}$	Average value of the lower arm capacitor voltages.
$u_{\rm diff}$	Inner difference voltage.
n_Δ	Difference of the arm inserted SM numbers.
n_Σ	Total arm inserted SM number.
$u_{\rm nom}$	Normalized ac-side output voltage.
T_0	Fundamental wave cycle.
u_r	Summation of the capacitor voltage ripples of the inserted SMs in one phase-leg.
λ	Changing value of the arm inserted SM number.
$n_{\Sigma\max}$	Maximum value of the total inserted SM number.
$n_{\Sigma\min}$	Minimum value of the total inserted SM number.
$\rm SW_n$	The accumulative summation value of the turn-on and turn-off actions of all upper switches in one phase-leg SMs.

Manuscript received June 27, 2019; revised October 29, 2019 and January 24, 2020; accepted March 7, 2020. Date of publication March 22, 2020; date of current version July 20, 2020. This work was supported in part by the National Key Research & Development Plan under Grant 2018YFB0905800 and in part by the Fundamental Research Funds for the Central Universities under Grant xzy022019005. Recommended for publication by Associate Editor Y. Tang. *(Corresponding authors: Xingxing Chen; Jinjun Liu.)*

The authors are with the State Key Lab of Electrical Insulation and Power Equipment School of Electrical Engineering, Xi'an Jiaotong University, Xi'an 710049, China (e-mail: xingxingchen@stu.xjtu.edu.cn; jjliu@mail.xjtu.edu.cn; shuguang.song.chine@gmail.com; oysd1989@stu.xjtu.edu.cn).

Color versions of one or more of the figures in this article are available online at http://ieeexplore.ieee.org.

Digital Object Identifier 10.1109/TPEL.2020.2982781

I. INTRODUCTION

COMPARED with conventional multilevel converters, such as neutral-point-clamped and flying-capacitor converters, the modular multilevel converter (MMC) features modularity, scalability, reduced voltage stress of power switches, and high quality of output waveforms [1]–[8]. Over the past decade, MMC has become one of the most promising topologies in high-voltage direct current transmission system [4], [5], and has also been applied to some medium voltage applications, such as motor

drive [6], static synchronous compensator (STATCOM) [7], and battery energy storage system [8].

The most commonly used modulation methods of the MMC are pulsewidth modulation (PWM) [9], [10] and nearest level modulation (NLM) [11], [12]. The PWM method produces lower total harmonics distortion, but is complicated to implement as the increasing of the MMC submodule (SM) number, since each SM should be equipped with a carrier waveform. In comparison, the NLM method has simple implementation and low switching frequency characteristic. To improve the quality of the ac-side output voltage, a level-increased NLM method is proposed in [13] and [14] to increase the maximum number of the ac-side output voltage levels to $2N + 1$, which is considered as the modulation method for the MMC in this article. Besides the ac-side output voltage levels, the performance differences of the MMC by using the NLM and level-increased NLM can be summarized as follows: 1) the transition edges of the upper and lower arm voltages are aligned with NLM, but they are unaligned with level-increased NLM; and 2) the total inserted SM number in one phase-leg of the MMC is fixed at N with NLM, but it varies among N, $N + 1$, and $N - 1$ with level-increased NLM [13], [14].

The interaction between the SM modulation command and the arm current can result in remarkable ripple on the SM capacitor voltage of the MMC [15]. The ripple leads to a mismatch between the dc-side supply voltage and the summation of the arm voltages, which in turn introduces even-order harmonic components in the circulating current [16], [17]. Such low-order harmonics flowing through the MMC phase-leg can increase system power losses, current stress on the power switches, and capacitor voltage ripples. For the MMC with level-increased NLM, the peak-to-peak value of the circulating harmonic currents can be even higher this has not been noted in the existing literatures but will be analyzed in this article.

The circulating harmonic currents can be suppressed to improve the system performance. Suppression strategies can be classified into two categories: indirect control approaches and direct control approaches. Indirect control approaches based on proportional integral (PI) controller [18], [19], nonideal proportional resonant (PR) controller [20], and repetitive controller [21], [22], are done by introducing a common mode component in the arm voltage references at the modulation stage [23]. The PI and nonideal PR controllers are only applicable to handle one frequency component of the circulating harmonic currents. The repetitive controller can deal with multiple harmonic components. All techniques in this family have relatively complicated design process. The parameters in these controllers are difficult to tune, and the dynamic performance is influenced by the bandwidth of the controllers [24]. The direct control approaches proposed in [25]–[29] are done by adjusting the total inserted SM number in one phase-leg of the MMC according to the instantaneous current information after the modulation stage. That kind of methods have simple implementation and high dynamic performance compared with indirect control approaches [25], [29], therefore, this article focuses mainly on direct control approaches.

Three important problems have not been well addressed in existing direct control methods. They are as follows.

1) The deviation of the circulating current from its reference can be large at the transient state, and the peak-to-peak value of the circulating harmonic currents will be high at the steady state as the operation voltage and power or the allowable capacitor voltage ripple of the MMC increases [30]. In those cases, the total inserted SM number in one phase-leg of the MMC should be extended to $N \pm \delta$ to improve the circulating current control performance at the dynamic and steady states, where N is the SM number per arm, and δ is an integer and can be larger than 10 at steady state as analyzed in [30]. In [25]–[29], no specific extension principle of the total inserted SM number is given to handle large circulating harmonic currents and only two total inserted SM numbers are considered besides N (Konstantinou *et al.* [25] mentioned that the total inserted SM number could be further extended according to the control requirement, however, no detailed extension principle or algorithm are given).
2) The circulating current control can disturb the quality of the ac-side output voltage. In [25], [26], [28], and [29], the total inserted SM numbers $N \pm 1$ are used to control the circulating current, which can affect the ac-side voltage level when the NLM is applied for the MMC. Instead, the total inserted SM numbers $N \pm 2$ are utilized in [27], and one additional SM is inserted or bypassed in both the upper and lower arms. Therefore, the quality of the ac-side output voltage remains unaffected for the NLM applied MMC, while regulating the circulating current. However, this method is only applicable for the MMC with a constant N of total inserted SM number. For the level-increased NLM applied MMC, the total inserted SM number is changed among $(N - 1, N, N + 1)$. By using the suppression methods in [25]–[28], the quality of the ac-side output voltage can still be disturbed.
3) The third problem is the combination of the first and second problems. That is when the total inserted SM number in one phase-leg of the MMC is extended to $N \pm \delta$ ($\delta \geq 2$), the adjustment principle of the total inserted SM number and the calculation of the arm inserted SM number to avoid disturbing the quality of the ac-side output voltage while regulating the circulating current has not been presented in [25]–[29].

In [27] and [28], the mechanism of the direct circulating current control approaches is analyzed in detail, and a hysteresis control method is proposed for the MMC with NLM. This article proposes improvements based on [27] and [28], which are listed as follows:

1) The effect of the level-increased NLM to the inner circulating current of the MMC is analyzed and it is observed that the peak-to-peak value of the circulating harmonic currents can be high when the level-increased NLM is used.
2) A general direct circulating harmonic currents suppression method is proposed for the MMC with NLM and

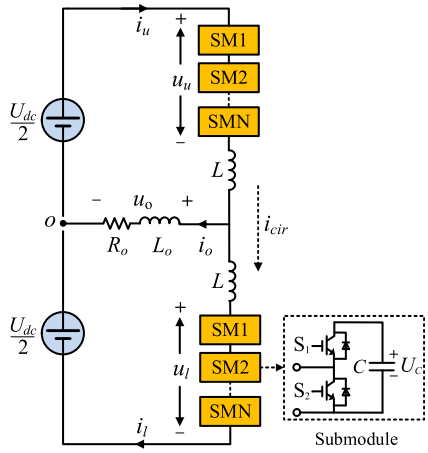

Fig. 1. Circuit configuration of single-phase MMC.

level-increased NLM by applying deadbeat control. However, only the situation with level-increased NLM is analyzed. The circulating harmonic currents suppression of the MMC with NLM can be regarded as a special case of the proposed circulating current control principle. The proposed method presents specific extension and adjustment principle of the total inserted SM number to improve the dynamic control performance, handle large circulating harmonic currents and avoid disturbing the ac-side output voltage while regulating the circulating current.

3) The effectiveness of the proposed method is verified through simulation and experiment.
4) Comprehensive simulation and experimental comparisons between the proposed method and one of the typical direct circulating current control method presented in [25] and [26] are given.

The reason why this method is chosen to do the comparison is that this method reflects all of the problems that the existing direct circulating current control methods have.

The rest of this article is organized as follows: Section II describes the basic structure of a single-phase MMC and the implementation of the level-increased NLM; Section III explains the effect of the level-increased NLM on the inner circulating current and presents the proposed circulating harmonic currents suppression method; Section IV and V show the simulation and experimental results, respectively. Finally, Section VI concludes this article.

II. Operation Principle of the MMC

A. Basic Structure

The basic structure of a single-phase MMC shown in Fig. 1 comprises an upper arm and a lower arm. Each arm includes *N* series-connected SMs and one buffer inductor *L*, where each SM is typically a half-bridge circuit. *C* is the SM capacitance. There are two states of the MMC SM under normal operating conditions. One is the inserted state, when the upper switch is turned ON and the lower switch is turned OFF. In this situation, the SM output voltage equals the capacitor voltage U_c. Another is the bypassed state, when the upper switch is turned OFF and the lower switch is turned ON. Then, the SM output voltage becomes zero. The dc-side of the converter is supplied by a dc voltage source $U_{\rm dc}$, which is equally distributed on the *N* SMs, therefore, the nominal average value of the SM capacitor voltage equals $U_{\rm dc}/N$. $R_{\rm o}$ and $L_{\rm o}$ are the load resistance and inductance, respectively. $u_{\rm o}$ is the load voltage.

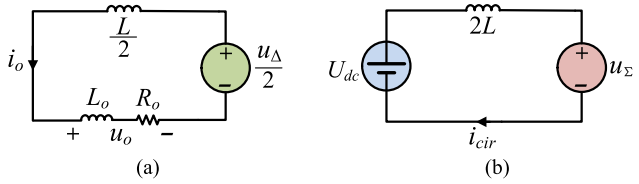

Fig. 2. Equivalent circuits of the MMC. (a) AC-side equivalent circuit. (b) Phase-leg equivalent circuit.

Applying Kirchhoff's current law, as shown in Fig. 1, the output current $i_{\rm o}$ and the circulating current $i_{\rm cir}$ can be given as

$$i_o = i_u - i_l \tag{1}$$

$$i_{\rm cir} = \frac{i_u + i_l}{2} = i_{\rm dc} + i_h \tag{2}$$

where i_u and i_l represent the upper arm current and lower arm current, respectively. $i_{\rm dc}$ is the dc component and i_h is the harmonic components of the circulating current.

The difference and summation of the arm voltages are expressed as

$$u_\Delta = u_l - u_u \tag{3}$$

$$u_\Sigma = u_l + u_u \tag{4}$$

where u_l and u_u are the lower arm and upper arm voltages, respectively. For an MMC system with well-balanced capacitor voltage, the arm voltages can be written as

$$u_u = n_u U_{\rm cu\_ave} \tag{5}$$

$$u_l = n_l U_{\rm cl\_ave} \tag{6}$$

where n_u and n_l are the inserted SM numbers in the upper and lower arms, respectively. $U_{\rm cu\_ave}$ and $U_{\rm cl\_ave}$ are the average capacitor voltages in the corresponding arm.

The ac-side and phase-leg equivalent circuits of the MMC are shown in Fig. 2 and the generalized mathematical model [18] is described as

$$\frac{u_\Delta}{2} = R_o i_o + \left(\frac{L}{2} + L_o\right)\frac{di_o}{dt} \tag{7}$$

$$\frac{u_\Sigma}{2} = \frac{U_{\rm dc}}{2} - L\frac{di_{\rm cir}}{dt}. \tag{8}$$

Fig. 2 shows that $u_\Delta/2$ is the equivalent ac-side output voltage driving the output current, and the inner difference voltage $u_{\rm diff}$ ($u_{\rm diff} = u_\Sigma - U_{\rm dc}$) drives the circulating current. The arm buffer inductance is *L*/2 from the point of view of the ac-side circuit.

The difference and total arm inserted SM numbers are denoted by n_Δ and n_Σ ($n_\Delta = n_l - n_u$ and $n_\Sigma = n_l + n_u$), respectively. Substituting (5) and (6) into (3) and ignoring the effect of the capacitor voltage ripples ($U_{\rm cu\_ave}$ and $U_{\rm cl\_ave}$ are equal to

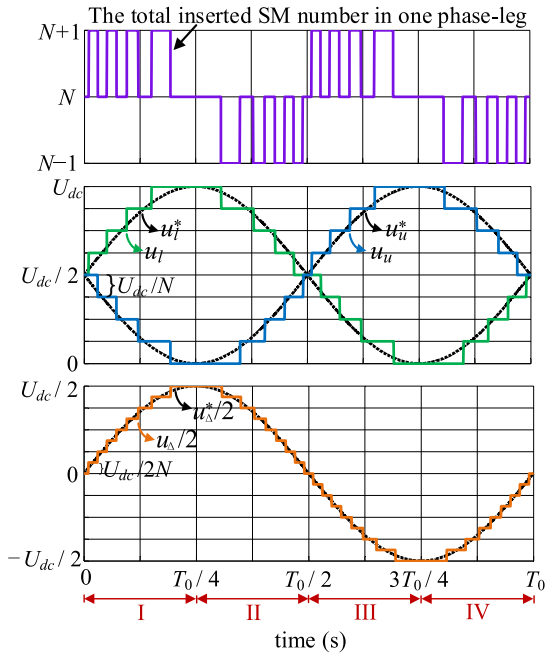

Fig. 3. Relevant waveforms of the MMC with level-increased NLM.

$U_{\rm dc}/N$) on the ac-side output voltage, the equivalent ac-side output voltage can be represented by the difference arm inserted SM number and can be given as

$$\frac{u_\Delta}{2} = \frac{n_l - n_u}{2}\frac{U_{\rm dc}}{N} = \frac{n_\Delta}{2}\frac{U_{\rm dc}}{N}. \tag{9}$$

According to (9), the corresponding normalized ac-side output voltage based on $U_{\rm dc}/N$ are [*N*/2, $(N-1)$/2,… 0…,–$(N-1)$/2, $-N$/2] with different combinations of the arm inserted SM numbers (n_l–$n_u = N$, $N-1$,…0, $-N+1$, $-N$). The normalized ac-side output voltage can be represented by the difference value of the arm inserted SM numbers and is given as

$$u_{\rm nom} = \frac{n_l - n_u}{2} = \frac{n_\Delta}{2}. \tag{10}$$

B. Level-Increased NLM

Fig. 3 shows the waveforms of the level-increased NLM based MMC with four SMs per arm ($N = 4$). T_0 is the fundamental wave cycle. $u_\Delta^*/2$ is the reference of the ac-side output voltage. u_u^* and u_l^* are the references of the arm voltages, which are written as [18]

$$u_u^* = \frac{U_{\rm dc} - u_\Delta^*}{2} \tag{11}$$

$$u_l^* = \frac{U_{\rm dc} + u_\Delta^*}{2}. \tag{12}$$

By applying the level-increased NLM [13], the arm inserted SM numbers are calculated as

$$n_u = \text{round}\left(\frac{Nu_u^*}{U_{\rm dc}} + y\right) \tag{13}$$

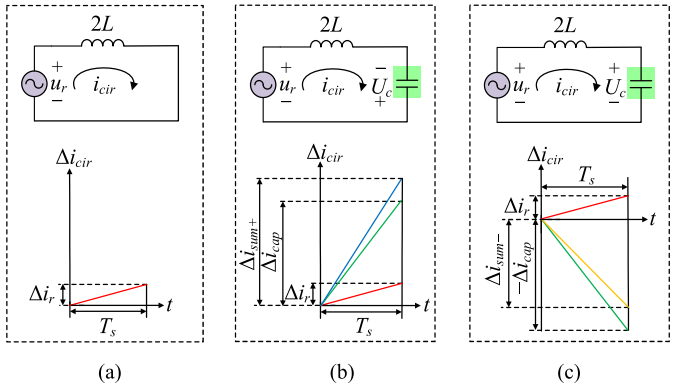

Fig. 4. Equivalent phase-leg circuits of the MMC with different total inserted SM numbers and the corresponding circulating current waveforms. (a) $n_\Sigma = N$. (b) $n_\Sigma = N-1$. (c) $n_\Sigma = N+1$.

$$n_l = \text{round}\left(\frac{Nu_l^*}{U_{\rm dc}} + y\right) \tag{14}$$

where *round* (x) returns the nearest integer of the real number x, for example, *round* $(5.4) = 5$ and *round* $(5.6) = 6$. For the NLM method, y is 0 and the total inserted SM number in one phase-leg of the MMC is fixed at N [13]. But for the level-increased NLM method, y alternates in a double fundamental frequency and can be expressed as

$$y = \begin{cases} 0.25 & u_\Delta^*/2 \text{ in region I or III} \\ -0.25 & u_\Delta^*/2 \text{ in region II or IV.} \end{cases} \tag{15}$$

If $u_\Delta^*/2$ is in region I ($0 \le u_\Delta^*/2 \le U_{\rm dc}/2$ and $u_\Delta^*/2$ is increasing) or in region III ($-U_{\rm dc}/2 \le u_\Delta^*/2 < 0$ and $u_\Delta^*/2$ is decreasing), y is equal to 0.25. If $u_\Delta^*/2$ is in region II ($0 \le u_\Delta^*/2 \le U_{\rm dc}/2$ and $u_\Delta^*/2$ is decreasing) or in region IV ($-U_{\rm dc}/2 \le u_\Delta^*/2 < 0$ and $u_\Delta^*/2$ is increasing), y is equal to -0.25. It is shown in Fig. 3 that the total inserted SM number is not fixed at N but varies among N, $N+1$, and $N-1$. The transition edges of the upper and lower arm voltages are unaligned with level-increased NLM and $2N+1$ voltage levels are generated. A more detailed description of the level-increased NLM method can be found in [13].

III. Proposed Circulating Harmonic Currents Suppression Method

A. Circulating Current Affected by Level-Increased NLM

The equivalent phase-leg circuits of the level-increased NLM based MMC with different total inserted SM numbers and the corresponding circulating current waveforms are shown in Fig. 4. When the total inserted SM number is N in the phase-leg, $u_{\rm diff}$ depends on only the capacitor voltage ripples of the inserted SMs and is equal to u_r (u_r represents the summation of the inserted SM capacitor voltage ripples in one phase-leg of the MMC). The circulating current waveform is shown in Fig. 4(a) in that situation, where it is regarded as a straight line in one control cycle T_s and u_r is assumed in its positive period. Therefore, the circulating current increment Δi_{cir} is equal to Δi_r ($\Delta i_r = u_r T_s/2L$).

When $N-1$ SMs are inserted in the phase-leg, it can be equivalent to an additional capacitor is connected to the circuit with positive polarity. The phase-leg equivalent circuit is depicted in Fig. 4(b). An extra positive increment $\Delta i_{\rm cap} = U_c T_s/2L$ is introduced by the additional capacitor, and as a result, the circulating current increment Δi_{cir} is equal to $\Delta i_r + \Delta i_{\rm cap}$. In contrast, when $N+1$ SMs are inserted in the phase-leg, on the contrary, it can be equivalent to an additional capacitor is connected to the circuit with negative polarity and the phase-leg equivalent circuit is shown in Fig. 4(c). In that case, the circulating current increment Δi_{cir} is equal to $\Delta i_r - \Delta i_{\rm cap}$.

The analysis indicates that the circulating current will be increased or decreased as the changing of the total inserted SM number in one phase-leg of the MMC with level-increased NLM, and the harmonic components of the circulating current not only depend on the capacitor voltage ripples but also are affected by the modulation stage. The simulation and experimental results given in this article will show that the peak-to-peak value of the circulating harmonic currents can be large for the MMC with level-increased NLM.

B. Implementation of the Proposed Method

The implementation of the proposed circulating harmonic currents suppression method is presented in this section. Through level-increased NLM, the obtained inserted SM numbers in the upper and lower arms are represented by n_{u1} and n_{l1}, respectively. The difference and total inserted SM numbers are denoted by $n_{\Delta 1}$ and $n_{\Sigma 1}$. The normalized ac-side output voltage level is written as $n_{\Delta 1}/2$ according to (10).

The discrete-time expression of (8) is deduced by using forward Euler method [30]

$$u_\Sigma(k) = U_{\rm dc} - \frac{2L}{T_s}[i_{\rm cir}(k+1) - i_{\rm cir}(k)] \tag{16}$$

where $u_\Sigma(k)$ is the arm summation voltage at control step k and $i_{\rm cir}(k)$ is the measured circulating current. $i_{\rm cir}(k+1)$ is the circulating current value at the next control step $k+1$. To regulate the circulating current to its reference at the next control instant, $i_{\rm cir}(k+1)$ is replaced by its reference $i^*_{\rm cir}(k+1)$ in (16) based on the deadbeat control principle [31]. $i^*_{\rm cir}(k+1)$ is obtained from the system energy balancing control [25] and the average capacitor voltage control [32]. Therefore, the optimal value of $u_\Sigma(k)$ can be calculated as

$$u^*_\Sigma(k) = U_{\rm dc} - \frac{2L}{T_s}[i^*_{\rm cir}(k+1) - i_{\rm cir}(k)]. \tag{17}$$

Accordingly, the total inserted SM number through the circulating current control stage is obtained as

$$n_{\Sigma 2} = {\rm int}\left[\frac{N u^*_\Sigma(k)}{U_{\rm dc}}\right] \tag{18}$$

int(x) returns the nearest integer that is smaller than x, for example, int(5.1) = 5 and int(5.6) = 5.

Until now, there have been two values of the total inserted SM number. The first value $n_{\Sigma 1}$ derived from the modulation stage, can be N, $N-1$ or $N+1$. The second value $n_{\Sigma 2}$ is calculated in (18) at the circulating current control stage. To avoid disturbing the quality of the ac-side output voltage while regulating the circulating current, which requires maintaining the normalized ac-side output voltage at $n_{\Delta 1}/2$, the same change of the inserted SM number should be applied to the upper and lower arms at the circulating current control stage, according to (10). For example, if n_{l1}, $n_{u1} = 5$, and $n_{\Delta 1}/2 = 0$. Then, the value of the arm inserted SM numbers are adjusted to control the circulating current ($n_{l2} = n_{l1} + \Delta n_l$, $n_{u2} = n_{u1} + \Delta n_u$). If the value of Δn_l and Δn_u are not the same, for example, $n_{l1}+1$ and $n_{u1}+2$ ($n_{\Sigma 2} = n_{\Sigma 1} + 3$), the normalized ac-side output voltage will change to -0.5 ($n_{\Delta 2}/2 \neq n_{\Delta 1}/2$) according to (10). But if the value of Δn_l and Δn_u are the same, for example, $n_{l1}+1$ and $n_{u1}+1$ ($n_{\Sigma 2} = n_{\Sigma 1} + 2$), the normalized ac-side output voltage remains at 0 ($n_{\Delta 2}/2 = n_{\Delta 1}/2$). It can be concluded that $n_{\Sigma 2}$ should be equal to $n_{\Sigma 1} \pm 2\lambda$, where λ is the changing value of the arm inserted SM number ($\lambda = 0, 1, 2 \ldots$). 2λ is an even value. Mathematically, any even number (odd number) adds or minus an even number still turns out an even number (odd number). Therefore, $n_{\Sigma 1}$ and $n_{\Sigma 2}$ should both be even numbers or odd numbers to avoid disturbing the quality of the ac-side output voltage while regulating the circulating current. Otherwise, $n_{\Sigma 2}$ calculated in (18) must be adjusted. Normally, N is designed as an even number [4], [6]–[8]. Therefore, $N-1$ and $N+1$ are odd numbers. The adjustment principle of $n_{\Sigma 2}$ is given as

$$n_{\Sigma 3} = \begin{cases} n_{\Sigma 2}+1 & n_{\Sigma 1} = N \ \& \ n_{\Sigma 2} \text{ is odd number} \\ n_{\Sigma 2} & n_{\Sigma 1} = N \ \& \ n_{\Sigma 2} \text{ is even number} \\ n_{\Sigma 2}+1 & n_{\Sigma 1} = N \pm 1 \ \& \ n_{\Sigma 2} \text{ is even number} \\ n_{\Sigma 2} & n_{\Sigma 1} = N \pm 1 \ \& \ n_{\Sigma 2} \text{ is odd number} \end{cases} \tag{19}$$

where $n_{\Sigma 3}$ is the obtained total inserted SM number after the adjustment. If $n_{\Sigma 1}$ is equal to N ($N \pm 1$) through level-increased NLM, and $n_{\Sigma 2}$ is an odd (even) number, $n_{\Sigma 3}$ should be equal to $n_{\Sigma 2}+1$, thus $n_{\Sigma 3}$ and $n_{\Sigma 1}$ will both be even (odd) numbers. If $n_{\Sigma 1}$ and $n_{\Sigma 2}$ are already both even or odd numbers, no change need to be applied to $n_{\Sigma 2}$ and $n_{\Sigma 3} = n_{\Sigma 2}$. $n_{\Sigma 2}$ is calculated by using int(x) function in (18). For example, if $N u^*_\Sigma(k)/U_{dc}$ in (18) equals 11.4, then $n_{\Sigma 2}+1$ and $n_{\Sigma 2}-1$ will equal 12 and 10, respectively. Compared with $n_{\Sigma 2}-1$, $n_{\Sigma 2}+1$ is closer to $N u^*_\Sigma(k)/U_{dc}$. Therefore, $n_{\Sigma 2}+1$ will be the optimal value to control the circulating current in (19-1). Similarly, $n_{\Sigma 2}+1$ will be the optimal value in (19–3).

To avoid a large *dv/dt* problem during a transient response, $n_{\Sigma 3}$ can be further restricted as

$$n_{\Sigma 3} = \begin{cases} N+\varepsilon & n_{\Sigma 3} \text{ is even number } \& \ n_{\Sigma 3} >= N+\varepsilon \\ N-\varepsilon & n_{\Sigma 3} \text{ is even number } \& \ n_{\Sigma 3} <= N-\varepsilon \\ N+\varepsilon-1 & n_{\Sigma 3} \text{ is odd number } \& \ n_{\Sigma 3} >= N+\varepsilon-1 \\ N-\varepsilon+1 & n_{\Sigma 3} \text{ is odd number } \& \ n_{\Sigma 3} <= N-\varepsilon+1 \end{cases} \tag{20}$$

ε is an even number and should not be smaller than $n_{\Sigma\max} - N$ and $N - n_{\Sigma\min}$, where $n_{\Sigma\max}$ and $n_{\Sigma\min}$ are the extreme values of the total inserted SM number to handle the circulating harmonic

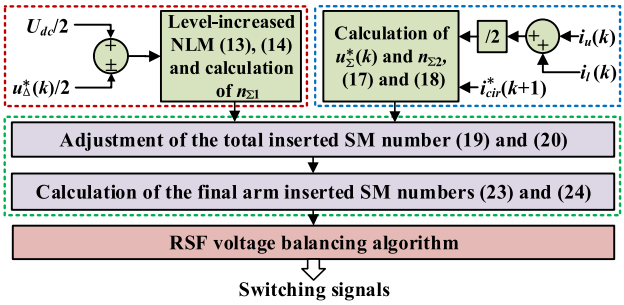

Fig. 5. Overall control structure of the MMC system with the proposed circulating harmonic currents suppression method.

TABLE I
PARAMETERS OF THE SIMULATION AND EXPERIMENT SYSTEMS

Parameter	Symbol	Simulation	Experiment
Dc-link voltage	U_{dc}	10 kV	210 V
SM number per arm	N	10	6
Fundamental frequency	f_o	50 Hz	50 Hz
Submodule capacitance	C	3.5 mF	2 mF
Arm inductance	L	10 mH	6 mH
Load inductance	L_o	10 mH	30 mH
Load resistance	R_o	20 Ω	15 Ω
Control cycle	T_s	100 μs	100 μs
Limitation value	ε	4	2

currents at the steady state, which can be calculated as [28]

$$n_{\Sigma\,\max} = \text{int}\left(\frac{V_{\text{dc}}}{U_{\text{dc}}/N - \Delta U_c}\right) \tag{21}$$

$$n_{\Sigma\,\min} = \text{ceil}\left(\frac{V_{\text{dc}}}{U_{\text{dc}}/N + \Delta U_c}\right) \tag{22}$$

where ceil (x) returns the nearest integer that is larger than x, for example, ceil(5.1) = 6 and ceil(5.6) = 6. ΔU_c is the allowable capacitor voltage ripple. If $n_{\Sigma 3}$ does not exceed the thresholds ($N+\varepsilon$, $N-\varepsilon$, $N+\varepsilon-1$ or $N-\varepsilon+1$) in (20), it will be equal to the original value obtained in (19). $n_{\Sigma 1}$ is the total inserted SM number obtained from the modulation stage and $n_{\Sigma 3}$ is the total inserted SM after considering the requirement of circulating current control. As mentioned above, the same change of the inserted SM number should be applied to the upper and lower arms at the circulating current control stage to avoid disturbing the ac-side output voltage. Therefore, the final values of the arm inserted SM numbers are calculated as

$$n_{\text{uf}} = n_{u1} + \frac{n_{\Sigma 3} - n_{\Sigma 1}}{2} \tag{23}$$

$$n_{\text{lf}} = n_{l1} + \frac{n_{\Sigma 3} - n_{\Sigma 1}}{2} \tag{24}$$

which means that $\lambda = (n_{\Sigma 3} - n_{\Sigma 1})/2$.

After deriving the arm inserted SM numbers, the reduced switching frequency capacitor voltage balancing algorithm proposed in [18] is used to output the switching signal for each SM. The overall control structure of the MMC with the proposed circulating harmonic currents suppression method is shown in Fig. 5.

The advantages of the proposed direct circulating current control method compared with the existing direct control methods for the MMC are summarized as follows.

1) The proposed control method can easily extend the total inserted SM number to $N \pm \delta$ ($\delta \geq 2$) by using deadbeat control as shown in (17) and (18). The practicality and motivation of using $\delta \geq 2$ can be explained in two aspects. The first aspect is to suppress large circulating harmonic currents at the steady state as the operation voltage and power or the allowable capacitor voltage ripple of the MMC increases; the second aspect is to handle large circulating current deviation and improve the response of circulating current control at dynamic state. A larger value of δ means that more additional capacitors will be connected to the phase-leg, therefore, Δi_{cap} can be increased to $\delta U_c T_s/2L$ to improve the performance of circulating current control.
2) The proposed control method can well coordinate the circulating current control and modulation stages, even when the total inserted SM number is extended to large value. Therefore, the quality of the ac-side output voltage will always not be disturbed while regulating the circulating current.
3) The proposed control method is applicable to MMC with both level-increased NLM and conventional NLM. Control of the circulating current for the NLM based MMC can be regarded as a special case of the proposed control principle, when $n_{\Sigma 1}$ and $n_{\Sigma 3}$ are always even numbers ($n_{\Sigma 1}$ always equals N for NLM based MMC).
4) Since the ac-side output voltage will not be affected while regulating the circulating current by using the proposed control method, different control frequencies can be used for the ac-side control and circulating current control loops. A controllable tradeoff between the circulating harmonic currents suppression and the average switching frequency of the switching devices, can be realized by adjusting the circulating current control frequency of the proposed method.
5) When the system parameters (U_{dc}, L, T_s) are changed, the proposed controller requires only a simple modification of the discrete-time (16), therefore, this method is flexible to be applied to different MMC systems. Some improved deadbeat control methods [33]–[35] can be applied to overcome the parameter sensitivity problem.

IV. INDUSTRIAL-LEVEL SIMULATION VALIDATION

A single-phase MMC simulated model shown in Fig. 1 is established in PSCAD/EMTDC software to demonstrate the theoretical analysis in this article and verify the effectiveness of the proposed circulating harmonic currents suppression method. Detailed system parameters are listed in Table I. The simulation results show the difference between the circulating harmonic currents of the MMC with NLM and level-increased NLM. They also compare the MMC system performance using the proposed method with one of the typical direct circulating current control methods given in [25] and [26] (called redundant

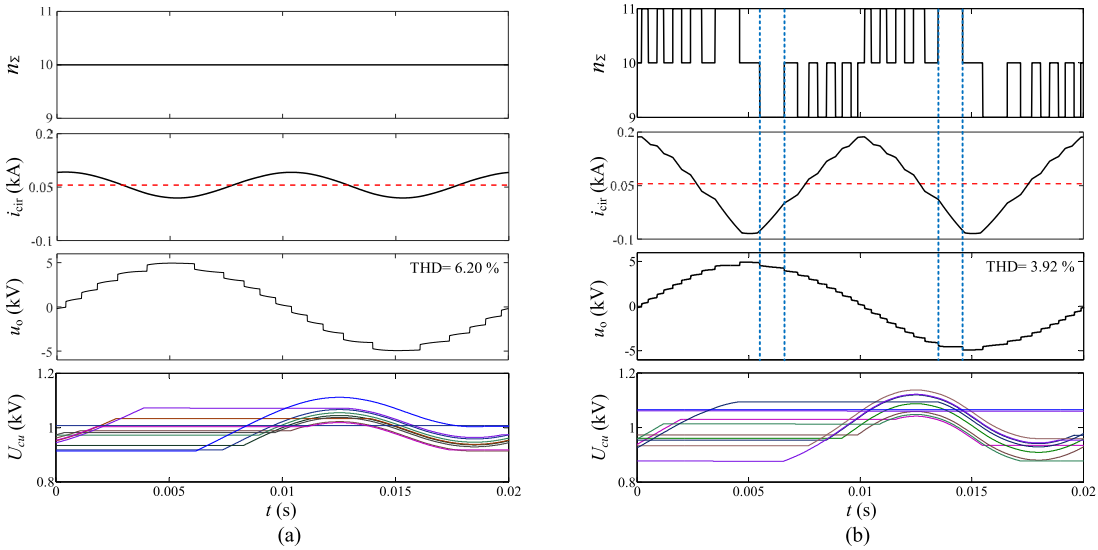

Fig. 6. One fundamental wave cycle of the MMC with (a) NLM; (b) level-increased NLM.

voltage level based method). The theoretical analysis focuses on the level-increased NLM based MMC in this article, but the simulation and experimental results present both NLM and level-increased NLM based MMC systems using the proposed circulating current control method.

One fundamental wave cycle of the NLM and level-increased NLM based MMC without circulating harmonic currents suppression are shown in Fig. 6(a) and (b), respectively. The number of the load voltage level is $N+1$ ($N=10$) and the total inserted SM number in one phase-leg of the MMC remains at N with NLM. In comparison, the number of the load voltage level is $2N+1$ and the total inserted SM number varies among $N-1$, N and $N+1$ with level-increased NLM. The red dotted line in the simulation figures is the dc reference of the circulating current. Note that the circulating current of the MMC performs mainly a dc plus second harmonic component with NLM, however, they are significantly affected by the modulation stage with level-increased NLM. When n_Σ equals $N-1$, the circulating current is increased as analyzed in Section III, and when n_Σ equals $N+1$, the circulating current is decreased. As the change of n_Σ, the peak-to-peak value of the circulating harmonic currents becomes considerable.

As mentioned before, the circulating current control of the MMC with NLM can be regarded as a special case of the proposed principle given in (19) and (20). Therefore, the effectiveness of the proposed method is first verified for the MMC with NLM and compared with the redundant voltage level based method. The simulation waveforms of the MMC using the redundant voltage level based method and the proposed method are shown in Fig. 7(a) and (b), respectively. The circulating harmonic currents suppression is enabled at 0.1 s. Both methods can well suppress the harmonic components of the circulating current. It is observed that n_Σ varies among 9, 10, and 11 using the redundant voltage level based method, however, n_Σ varies among 8, 10, and 12 using the proposed method at the steady state. The quality of the load voltage deteriorates using the redundant voltage level based method, however, it is improved slightly by using the proposed method. The capacitor voltage ripples are reduced after suppressing the circulating harmonic currents. The accumulative summation value of the turn-ON and turn-OFF actions of all upper switches in one phase-leg SMs (SW_n) using each of the two methods are also compared. The increasing slope of SW_n depends on the modulation stages before 0.1 s and increases somewhat after the circulating current control is enabled. And the increasing slope of SW_n in Fig. 7(a) is larger than that in Fig. 7(b). That is because the redundant voltage level based controller always transits to a nonredundant state ($n_\Sigma=9$, 11) after the redundant state ($n_\Sigma=10$) based on the control principle that if $i_{\mathrm{cir}} > i^*_{\mathrm{cir}}$ or $i_{\mathrm{cir}} < i^*_{\mathrm{cir}}$ [25]. But for the proposed method, the controller takes actions only when the circulating current exceeds certain values [27]. The zoomed-in transient state waveforms are shown in Fig. 8. The total inserted SM number is extended to 14 by using the proposed method, therefore, the reduction speed of the circulating current is faster than by using the redundant voltage level based method and the dynamic response is better.

For the level-increased NLM based MMC, the simulation waveforms are shown in Fig. 9(a) and (b), by enabling the two suppression methods at 0.1 s. The modulation and the circulating current control stages are not well coordinated by using the redundant voltage level based method, therefore, the quality of the load voltage deteriorates and the peak-to-peak value of the circulating harmonic currents is large than that of the proposed method after the controller is enabled. The quality of the load voltage is improved some by using the proposed method, and the circulating harmonic currents are well suppressed. The capacitor voltage ripples are also reduced after enabling the suppression.

The average switching frequency (f_{sw}) of the switching device in the MMC can be calculated by using (25) in the appendix. In Fig. 7, the value of f_{sw} using the proposed method is much smaller than using the redundant voltage level based method [$f_{\mathrm{sw}}=200$ Hz in Fig. 7(a) and $f_{\mathrm{sw}}=132$ Hz in Fig. 7(b)].

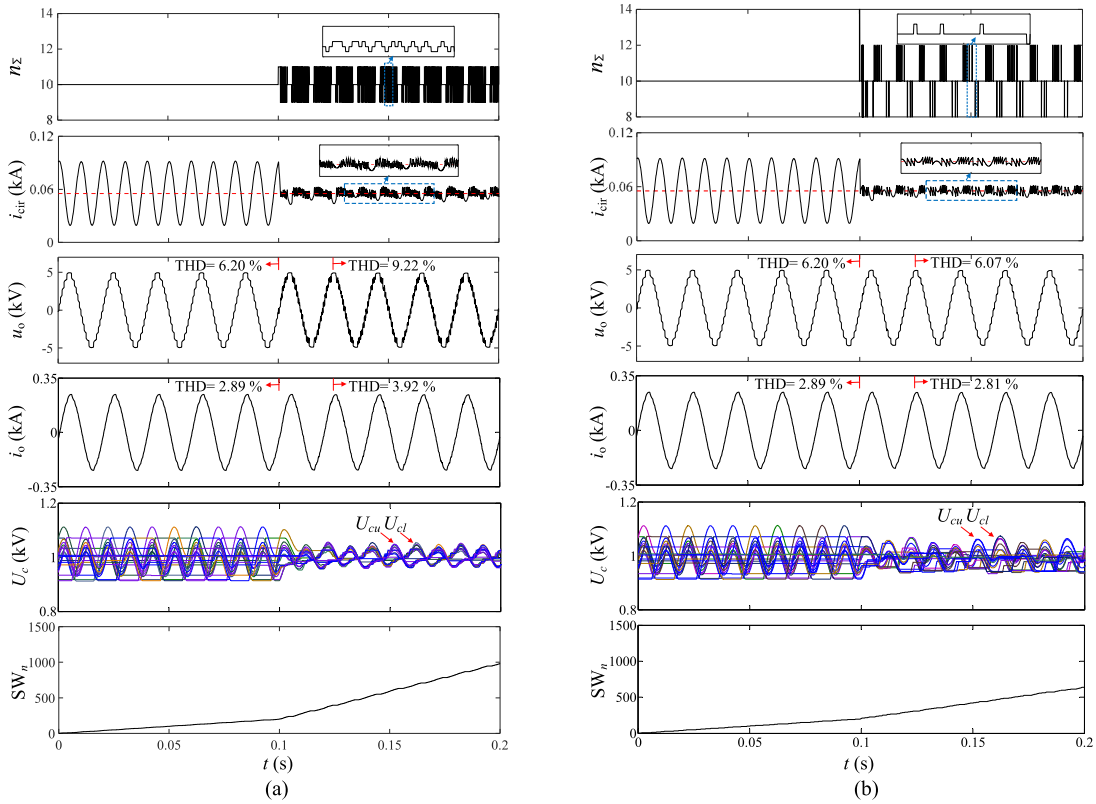

Fig. 7. Simulation waveforms of the NLM based MMC using (a) the redundant voltage level based method and (b) the proposed method.

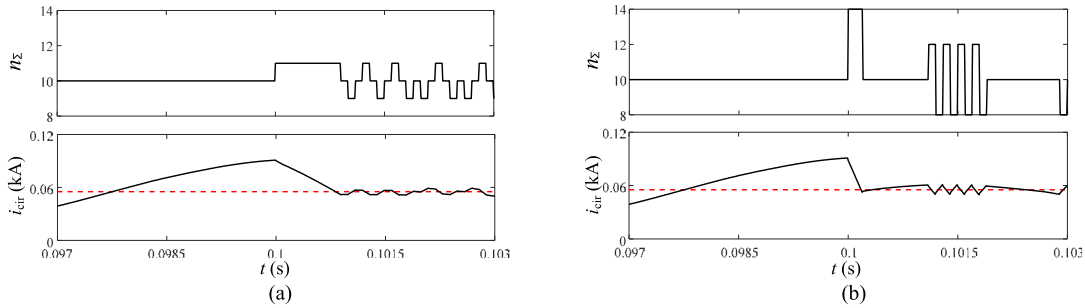

Fig. 8. Zoomed-in waveforms of the NLM based MMC using (a) the redundant voltage level based method and (b) the proposed method.

In Fig. 9, the value of f_{sw} after enabling the proposed method is larger than after enabling the redundant voltage level based method [$f_{sw} = 236$ Hz in Fig. 9(a) and $f_{sw} = 275$ Hz in Fig. 9(b)]. However, the peak-to-peak value of the circulating harmonic currents after enabling the suppression in Fig. 9(a) (28A) is larger than that in Fig. 9(b) (12A). The circulating current control frequency for both two methods in Fig. 9 is 10 kHz.

Since the ac-side output voltage will not be affected while regulating the circulating current by using the proposed control method, different control frequencies can be used for the ac-side control and circulating current control loops. If the circulating current control frequency for the proposed suppression method is reduced to 4 kHz, the peak-to-peak value of the circulating harmonic currents after enabling the suppression will also be 28 A, as shown in Fig. 10. In that situation, the value of f_{sw} is reduced to 113.75 Hz and is much smaller than that in Fig. 9(a). The simulation results by using the proposed suppression method with different peak-to-peak values of the circulating harmonic currents are summarized in Table II. It can be observed that, a controllable tradeoff between the circulating harmonic currents suppression and the average switching frequency of the switching devices in the MMC, can be realized by adjusting the circulating current control frequency of the proposed method.

V. Laboratory Experimental Validation

A down-scaled single-phase MMC prototype shown in Fig. 11 is built to verify the effectiveness of the proposed method. The detailed system parameters are listed in Table I. The control,

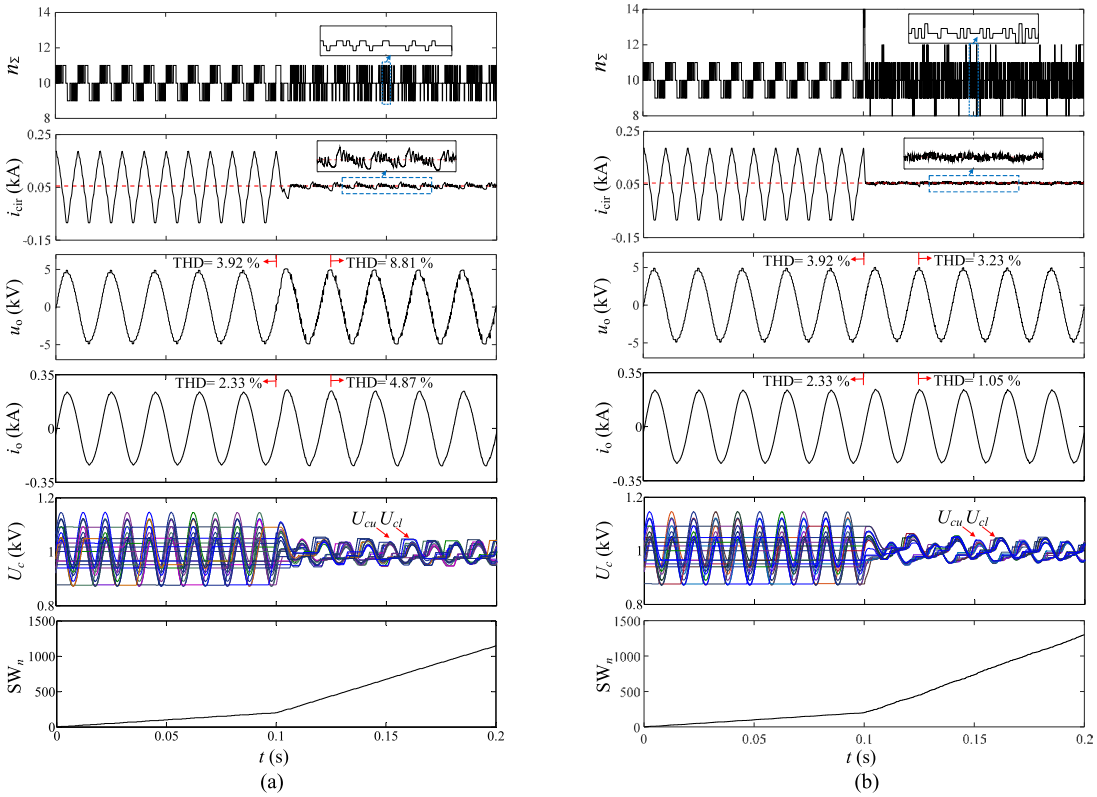

Fig. 9. Simulation waveforms of the level-increased NLM based MMC using (a) the redundant voltage level based method and (b) the proposed method.

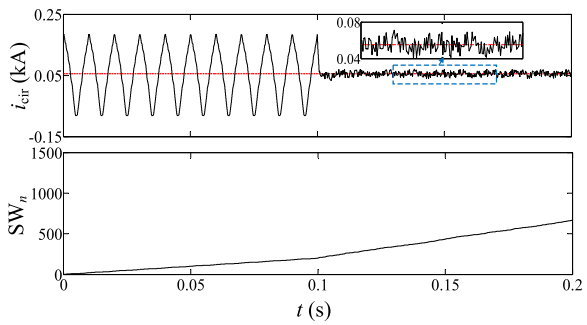

Fig. 10. Simulation waveforms of the level-increased NLM based MMC using the proposed suppression method with 4 kHz control frequency.

driving, and measurement algorithm is implemented with the digital control system Myway PE-Expert4.

The experimental waveforms of the MMC using NLM and level-increased NLM without circulating current control are shown in Fig. 12(a) and (b), respectively. $N + 1$ ($N = 6$) and $2N + 1$ load voltage levels are generated using NLM and level-increased NLM, respectively. The red dotted line in the experimental figures is the dc reference of the circulating current. The circulating current performs mainly a dc plus second harmonic component with NLM, however, they are significantly affected by the modulation with level-increased NLM and have larger peak-to-peak value.

For the NLM based MMC, the experimental waveforms are shown in Fig. 13(a) and (b), respectively, by using the redundant voltage level based method [25], [26] and the proposed method. The circulating harmonic currents suppression is enabled at 0.1 s. The harmonic components of the circulating current can be well suppressed by using both methods. The quality of the load voltage deteriorates using the redundant voltage level based method, however, it is improved slightly by using the proposed method. The capacitor voltage ripples are reduced after enabling the circulating harmonic currents suppression. The experimental results are identical with the simulation results.

TABLE II
ADJUSTMENT OF THE CONTROL FREQUENCY OF THE PROPOSED SUPPRESSION METHOD

The modulation method is NLM		
Peak-to-peak value of i_h	**Control frequency**	**Average switching frequency**
35 A	3 kHz	70 Hz
30 A	4 kHz	73 Hz
24 A	5 kHz	77 Hz
11 A	10 kHz	112 Hz
The modulation method is Level-Increased NLM		
Peak-to-peak value of i_h	**Control frequency**	**Average switching frequency**
38 A	3 kHz	83 Hz
28 A	4 kHz	115 Hz
21 A	5 kHz	135 Hz
10 A	10 kHz	276 Hz

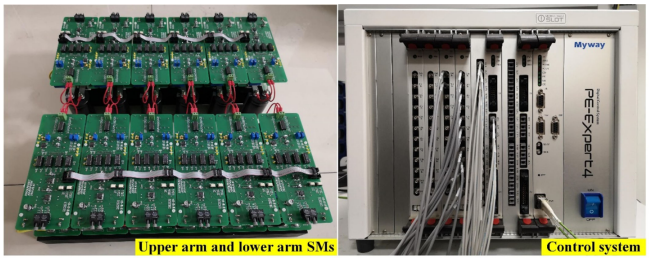

Fig. 11. Photograph of the single-phase MMC prototype. (a) Main circuit. (b) Digital control system Myway PE-Expert4.

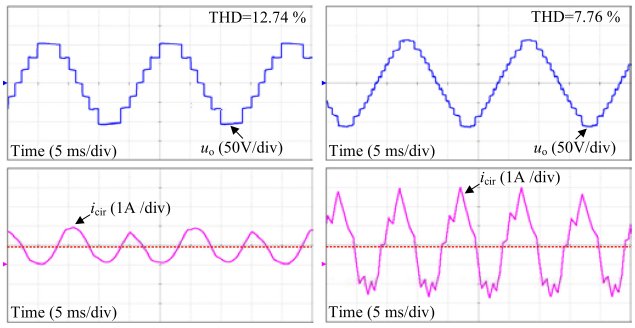

Fig. 12. Experimental results of the MMC with (a) NLM. (b) Level-increased NLM. From top to bottom: load voltage u_o, circulating current i_{cir}.

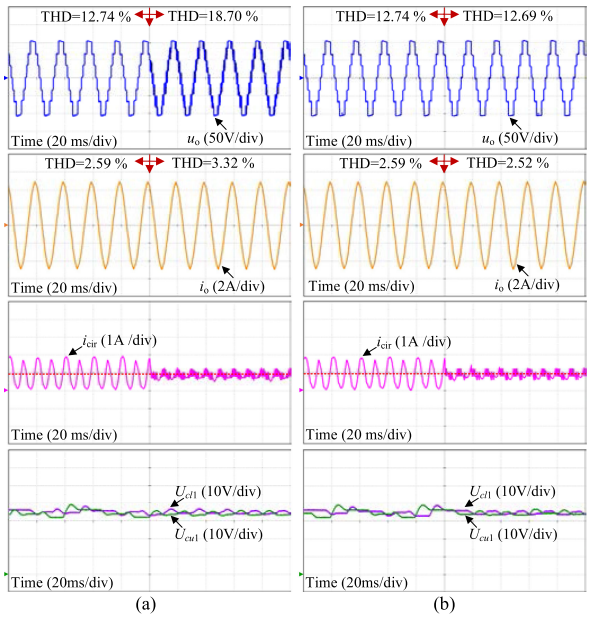

Fig. 13. Experimental results of the NLM based MMC using the (a) the redundant voltage level based method. (b) The proposed circulating harmonic currents suppression method. From top to bottom: load voltage u_o, ac-side output current i_o, circulating current i_{cir}, the first SM capacitor voltages in the upper and lower arms U_{cu1} and U_{cl1}.

For the level-increased NLM based MMC, the experimental waveforms are shown in Fig. 14(a) and (b), respectively, by enabling the redundant voltage level based method [25], [26] and the proposed method at 0.1 s. The quality of the load voltage deteriorates using the redundant voltage level based method

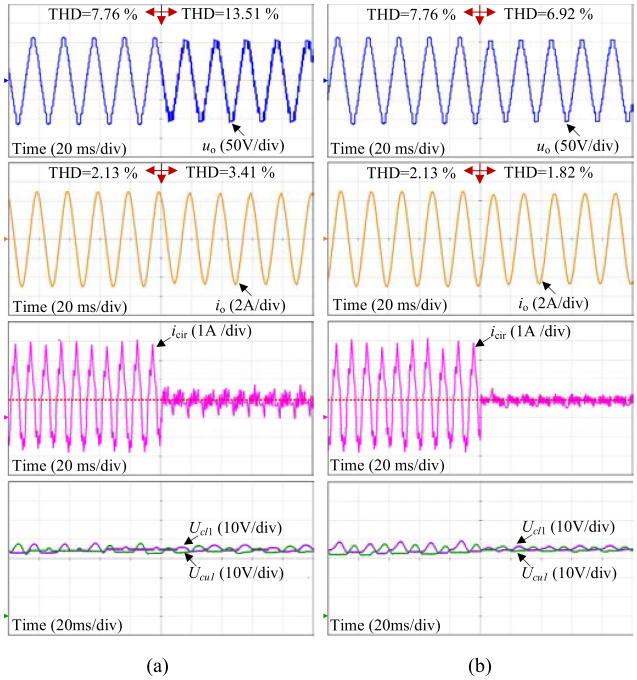

Fig. 14. Experimental results of the level-increased NLM based MMC using the (a) the redundant voltage level based method. (b) The proposed circulating harmonic currents suppression method. From top to bottom: load voltage u_o, ac-side output current i_o, circulating current i_{cir}, the first SM capacitor voltages in the upper and lower arms U_{cu1} and U_{cl1}.

and the peak-to-peak value of the circulating harmonic currents is large than that of the proposed method after the controller is enabled. The quality of the load voltage is improved some by using the proposed method. Similarly, the capacitor voltage ripples are reduced after 0.1 s.

VI. Conclusion

First, this article describes the effect of the level-increased NLM on the circulating current. As the changing of the total inserted SM number in one phase-leg of the MMC with level-increased NLM, the peak-to-peak value of the circulating current will become large. Second, a general circulating harmonic currents suppression method is proposed by applying deadbeat control, for the NLM and level-increased NLM based MMC. Then extension and adjustment principle for the total inserted SM number is presented. The purpose of the principle is to improve the dynamic control performance, handle large circulating harmonic currents at steady state and avoid disturbing the quality of the output waveforms while regulating the circulating current. Finally, in the simulation and experiment sections, the effectiveness of the proposed method is verified by a single-phase MMC prototype. A comprehensive comparison of the proposed method and one typical circulating current control method is also presented.

Appendix

In this part, some symbols are defined as follows:

$\boldsymbol{SW_n}$: The accumulative summation value of the turn-ON and turn-OFF actions of all upper switches in one phase-leg SMs.

$\boldsymbol{SW_{n''}}$: The accumulative summation value of the turn-ON and turn-OFF actions of all lower switches in one phase-leg SMs.

$\boldsymbol{f_{sw}}$: The average switching frequency of the switching device in the MMC.

The average switching frequency of the switching device is defined as: the average switching actions in 1 s. One complete switching action is regarded as one turn-ON action plus one turn-OFF action.

The value of $f_{\rm sw}$ in the simulation after 0.1 s (the circulating harmonic currents suppression is enabled at 0.1 s in Figs. 7 and 9) can be calculated step by step, as shown as follows:

1) The turn-ON and turn-OFF actions of all upper switches in one phase-leg SMs during 0.1 to 0.2 s in Figs. 7 and 9 equals $[\mathrm{SW}_n\,(t = 0.2\,\mathrm{s}) - \mathrm{SW}_n(t = 0.1\,\mathrm{s})]$. SW_n equals $\mathrm{SW}_{n''}$ for the MMC, because the upper and lower switches in one SM is complementary. In this article, SW_n is measured in the simulation and is used to calculate the value of f_{sw}.
2) The turn-ON and turn-OFF actions of all upper switches in the upper arm SMs equals that in the lower arm SMs during 0.1 to 0.2 s. Because the operation of the two arms are normally symmetrical. Therefore, the turn-ON and turn-OFF actions of all upper switches in one arm SMs during 0.1 to 0.2 s equals $[\mathrm{SW}_n(t = 0.2\,\mathrm{s}) - \mathrm{SW}_n(t = 0.1\,\mathrm{s})]/2$.
3) As mentioned above, one complete switching action is regarded as one turn-ON action plus one turn-OFF action, therefore, the switching actions of all upper switches in one arm SMs during 0.1 to 0.2 s equals $[\mathrm{SW}_n(t = 0.2\,\mathrm{s}) - \mathrm{SW}_n(t = 0.1\,\mathrm{s})]/4$ (the average turn-ON and turn-OFF actions for a switching device are usually the same in multiple fundamental cycles).
4) The switching actions of all upper switches in one arm SMs per second equals $10[\mathrm{SW}_n(t = 0.2\,\mathrm{s}) - \mathrm{SW}_n(t = 0.1\,\mathrm{s})]/4$.
5) The switching actions of the upper switch in every SM are the same if the parameters of the SMs are the same. There are 10 SMs per arm of the simulated MMC circuit, therefore, the average switching frequency of every switching device in one arm can be finally calculated as

$$f_{\rm sw} = \frac{\mathrm{SW}_n(t = 0.2\mathrm{s}) - \mathrm{SW}_n(t = 0.1\mathrm{s})}{4}. \tag{25}$$

REFERENCES

[1] A. Lesnicar and R. Marquardt, "An innovative modular multilevel converter topology suitable for a wide power range," in *Proc. IEEE Bologna Power Tech. Conf.*, Jun. 2003.

[2] S. Debnath, J. Qin, B. Bahrani, M. Saeedifard, and P. Barbosa, "Operation, control, and application of the modular multilevel converter: A review," *IEEE Trans. Power Electron.*, vol. 30, no. 1, pp. 37–53, Jan. 2015.

[3] A. Dekka, B. Wu, R. L. Fuentes, M. Perez, and N. R. Zargari, "Evolution of topologies, modeling, control schemes, and applications of modular multilevel converters," *IEEE J. Emerg. Sel. Topics Power Electron.*, vol. 5, no. 4, pp. 1631–1656, Dec. 2017.

[4] X. Shi *et al.*, "Characteristic investigation and control of modular multilevel converter-based HVDC system under single-line -to-ground fault conditions," *IEEE Trans. Power Electron.*, vol. 30, no. 1, pp. 408–421, Jan. 2015.

[5] A. Nami, J. Liang, F. Dijkhuizen, and G. D. Demetriades, "Modular multilevel converters for HVDC applications: Review on converter cells and functionalities," *IEEE Trans. Power Electron.*, vol. 30, no. 1, pp. 18–36, Jan. 2015.

[6] Y. Okazaki *et al.*, "Experimental comparisons between modular multilevel DSCC inverters and TSBC converters for medium-voltage motor drives," *IEEE Trans. Power Electron.*, vol. 32, no. 3, pp. 1805–1817, Mar. 2017.

[7] S. Du and J. Liu, "A study on DC voltage control for chopper-cell-based modular multilevel converters in D-STATCOM application," *IEEE Trans. Power Del.*, vol. 28, no. 4, pp. 2030–2038, Oct. 2013.

[8] T. Soong and P. W. Lehn, "Assessment of fault tolerance in modular multilevel converters with integrated energy storage," *IEEE Trans. Power Electron.*, vol. 31, no. 6, pp. 4085–4095, Jun. 2016.

[9] Z. Li, P. Wang, H. Zhu, Z. Chu, and Y. Li, "An improved pulse width modulation method for chopper-cell-based modular multilevel converters," *IEEE Trans. Power Electron.*, vol. 27, no. 8, pp. 3472–3481, Aug. 2012.

[10] B. Li, R. Yang, D. Xu, G. Wang, W. Wang, and D. Xu, "Analysis of the phase-shifted carrier modulation for modular multilevel converters," *IEEE Trans. Power Electron.*, vol. 30, no. 1, pp. 297–310, Jan. 2015.

[11] Q. Tu and Z. Xu, "Impact of sampling frequency on harmonic distortion for modular multilevel converter," *IEEE Trans. Power Del.*, vol. 26, no. 1, pp. 298–306, Jan. 2011.

[12] P. M. Meshram and V. B. Borghate, "A simplified nearest level control (NLC) voltage balancing method for modular multilevel converter (MMC)," *IEEE Trans. Power Electron.*, vol. 30, no. 1, pp. 450–462, Jan. 2015.

[13] L. Lin, Y. Lin, Z. He, Y. Chen, J. Hu, and W. Li, "Improved nearest-level modulation for a modular multilevel converter with a lower submodule number," *IEEE Trans. Power Electron.*, vol. 31, no. 8, pp. 5369–5377, Aug. 2016.

[14] P. Hu and D. Jiang, "A level-increased nearest level modulation method for modular multilevel converter," *IEEE Trans. Power Electron.*, vol. 30, no. 4, pp. 1836–1842, Apr. 2015.

[15] K. Ilves, A. Antonopoulos, S. Norrga, and H. P. Nee, "Steady-state analysis of interaction between harmonic components of arm and line quantities of modular multilevel converters," *IEEE Trans. Power Electron.*, vol. 27, no. 1, pp. 57–68, Jan. 2012.

[16] B. Chen, Y. Chen, C. Tian, J. Yuan, and X. Yao, "Analysis and suppression of circulating currents in a modular multilevel converter considering the impact of dead time," *IEEE Trans. Power Electron.*, vol. 30, no. 7, pp. 3542–3552, Jul. 2015.

[17] J. Sun and H. Liu, "Sequence impedance modeling of modular multilevel converters," *IEEE J. Emerg. Sel. Topics Power Electron.*, vol. 5, no. 4, pp. 1427–1443, Dec. 2017.

[18] Q. Tu, Z. Xu, and L. Xu, "Reduced switching-frequency modulation and circulating current suppression for modular multilevel converters," *IEEE Trans. Power Del.*, vol. 26, no. 3, pp. 2009–2017, Jul. 2011.

[19] B. Bahrani, S. Debnath, and M. Saeedifard, "Circulating current suppression of the modular multilevel converter in a double-frequency rotating reference frame," *IEEE Trans. Power Electron.*, vol. 31, no. 1, pp. 783–792, Jan. 2016.

[20] S. Li, X. Wang, Z. Yao, T. li, and Z. Peng, "Circulating current suppressing strategy for MMC-HVDC based on nonideal proportional resonant controllers under unbalanced grid conditions," *IEEE Trans. Power Electron.*, vol. 30, no. 1, pp. 387–397, Jan. 2015.

[21] L. He, K. Zhang, J. Xiong, and S. Fan, "A repetitive control scheme for harmonic suppression of circulating current in modular multilevel converter," *IEEE Trans. Power Electron.*, vol. 30, no. 1, pp. 471–481, Jan. 2015.

[22] S. Yang, P. Wang, Y. Tang, M. Zagrodnik, X. Hu, and K. J. Tseng, "Circulating current suppression in modular multilevel converters with even-harmonic repetitive control," *IEEE Trans. Ind. Appl.*, vol. 5544, no. 1, pp. 298–309, Jan. 2018.

[23] Y. Li, E. A. Jones, and F. Wang, "Circulating current suppressing control's impact on arm inductance selection for modular multilevel converter," *IEEE J. Emerg. Sel. Topics Power Electron.*, vol. 5, no. 1, pp. 182–188, Mar. 2017.

[24] A. Dekka, B. Wu, V. Yaramasu, and N. R. Zargari, "Dual-stage model predictive control with improved harmonic performance for modular multilevel converter," *IEEE Trans. Ind. Electron.*, vol. 63, no. 10, pp. 6010–6019, Oct. 2016.

[25] G. Konstantinou, J. Pou, S. Ceballos, R. Picas, J. Zaragoza, and V. G. Agelidis, "Control of circulating currents in modular multilevel converters through redundant voltage levels," *IEEE Trans. Power Electron.*, vol. 31, no. 11, pp. 7761–7769, Nov. 2016.
[26] G. Konstantinou, J. Pou, S. Ceballos, R. Picas, J. Zaragoza, and V. G. Agelidis, "Utilising redundant voltage levels for circulating current control in modular multilevel converters" in *Proc. 41st Annu. Conf. IEEE Ind. Electron. Soc.*, Nov. 2015, pp. 002213–002218.
[27] X. Chen, J. Liu, S. Ouyang, and S. Song, "A modified circulating current suppressing strategy for nearest level control based modular multilevel converter," in *Proc. IEEE Energy Convers. Congr. Expo. Conf.*, Sep. 2017, pp. 1817–1822.
[28] X. Chen, J. Liu, S. Ouyang, and S. Song, "An improved circulating current control strategy for modular multilevel converters through redundant voltage levels" in *Proc. IEEE 2nd Annu. Southern Power Electron. Conf.*, Dec. 2016, pp. 1–4.
[29] A. P. Basante, S. Ceballos, G. Konstantinou, J. Pou, J. Andreu, and I. M. de Alegría, "$(2N + 1)$ selective harmonic elimination-PWM for modular multilevel converters: A generalized formulation and a circulating current control method," *IEEE Trans. Power Electron.*, vol. 33, no. 1, pp. 802–818, Jan. 2018.
[30] F. Zhang, W. Li, and G. Joós, "A voltage-level-based model predictive control of modular multilevel converter," *IEEE Trans. Ind. Electron.*, vol. 63, no. 8, pp. 5301–5312, Aug. 2016.
[31] O. Kükrer, "Deadbeat control of a three-phase inverter with an output LC filter," *IEEE Trans. Power Electron.*, vol. 11, no. 1, pp. 16–23, Jan. 1996.
[32] M. Hagiwara and H. Akagi, "Control and experiment of pulsewidth-modulated modular multilevel converters," *IEEE Trans. Power Electron.*, vol. 24, no. 7, pp. 1737–1746, Jul. 2009.
[33] Y. A. I. Mohamed and E. F. Saadany, "An improved deadbeat current control scheme with a novel adaptive self-tuning load model for a three-phase PWM voltage-source inverter," *IEEE Trans. Ind. Electron.*, vol. 54, no. 2, pp. 747–759, Apr. 2007.
[34] J. M. Espí, J. Castelló, R. G. Gil, G. Garcerá, and E. Figueres, "An adaptive robust predictive current control for three-phase grid-connected inverters," *IEEE Trans. Ind. Electron.*, vol. 58, no. 8, pp. 3537–3546, Aug. 2011.
[35] G. H. Bode, P. C. Loh, M. J. Newman, and D. G. Holmes, "An improved robust predictive current regulation algorithm," *IEEE Trans. Power Electron.*, vol. 41, no. 6, pp. 1720–1773, Nov. 2005.

Xingxing Chen (Student Member, IEEE) received the B.S. degree in electrical engineering from Southwest Jiaotong University, Chengdu, China, in 2015. He is currently working toward the Ph. D. degree with Xi'an Jiaotong University, Xi'an, China.

His current research interests include multilevel converters, converter modeling, and control techniques.

Jinjun Liu (Fellow, IEEE) received the B.S. and Ph.D. degrees in electrical engineering from Xi'an Jiaotong University (XJTU), Xi'an, China, in 1992 and 1997, respectively.

He then joined the XJTU Electrical Engineering School as a Faculty. From late 1999 to early 2002, he was with the Center for Power Electronics Systems, Virginia Polytechnic Institute and State University, Blacksburg, VA, USA, as a Visiting Scholar. In late 2002, he was promoted to a Full Professor and then the Head of the Power Electronics and Renewable Energy Center with XJTU, which now comprises 17 faculty members and over 100 graduate students and carries one of the leading power electronics programs in China. From 2005 to early 2010, he served as an Associate Dean with Electrical Engineering School, XJTU, and from 2009 to early 2015, the Dean with Undergraduate Education, XJTU. He is currently a XJTU Distinguished Professor of Power Electronics, sponsored by Chang Jiang Scholars Program of Chinese Ministry of Education. He has coauthored three books (including one textbook), authored/coauthored more than 400 technical papers in peer-reviewed journals and conference proceedings, holds nearly 50 invention patents (China/US), and delivered for many times plenary keynote speeches and tutorials at IEEE conferences or China national conferences in power electronics area. His research interests include power quality control and utility applications of power electronics, microgrids for sustainable energy and distributed generation, and more/all electronic power systems.

Dr. Liu received for eight times governmental awards at national level or provincial/ministerial level for scientific research/teaching achievements. He was also a recipient of the 2006 Delta Scholar Award, the 2014 Chang Jiang Scholar Award, the 2014 Outstanding Sci-Tech Worker of the Nation Award, and the IEEE Transactions on Power Electronics 2016 Prize Paper Award. He was the IEEE Power Electronics Society Region 10 Liaison and then China Liaison for 10 years, an Associate Editor for the IEEE TRANSACTIONS ON POWER ELECTRONICS for 12 years, and from early 2015, the Vice President for membership of IEEE PELS. He is on the Board of China Electrotechnical Society and was elected the Vice President of the CES Power Electronics Society in 2013. Since 2013, he has been the Vice President for International Affairs, China Power Supply Society (CPSS) and since 2016, the inaugural Editor-in-Chief of CPSS Transactions on Power Electronics and Applications. Since 2013, he has been serving as the Vice Chair of the Chinese National Steering Committee for College Electric Power Engineering Programs.

Shuguang Song (Student Member, IEEE) received the B.S. degree in electrical engineering in 2014 from Xi'an Jiaotong University, Xi'an, China, where he is currently working toward the Ph.D. degree in electrical engineering.

His current research interests include multilevel converters in power quality, HVdc, and motor drive applications.

Shaodi Ouyang (Member, IEEE) received the B.S. degree from the Huazhong University of Science and Technology, Wuhan, China, in 2011, and the Ph.D degree from Xi'an Jiaotong University, Xi'an, China, in 2018, both in electrical engineering.

In 2019, he joined Xi'an Jiaotong University, as an Assistant Research Accociate. His research interests include power electronic transformer, multilevel converters, and dc–dc converters.